doi:10.1093/brain/aws092 Brain 2012: 135; 1606–1621 | 1606

BRAIN
A JOURNAL OF NEUROLOGY

Disrupted surface cross-talk between NMDA and Ephrin-B2 receptors in anti-NMDA encephalitis

Lenka Mikasova,[1,2] Pierre De Rossi,[3,4] Delphine Bouchet,[1,2] François Georges,[1,2] Véronique Rogemond,[3,4,5] Adrien Didelot,[3,4,5] Claire Meissirel,[3,4] Jérôme Honnorat[3,4,5] and Laurent Groc[1,2]

1 Interdisciplinary Institute for Neuroscience, Universite de Bordeaux, UMR 5297, F-33000 Bordeaux, France
2 CNRS, IINS, F-33000 Bordeaux, France
3 Lyon Neuroscience Research Centre, INSERM U1028/CNRS UMR 5292, F-69372 Lyon, France
4 Université de Lyon, Université Claude Bernard Lyon 1, F-69372 Lyon, France
5 Hospices Civils de Lyon, Hôpital Neurologique, Centre de Référence Maladie Rare 'Syndromes neurologiques Paranéoplasiques', F-69677 Bron, France

Correspondence to: Laurent Groc,
CNRS, Interdisciplinary Institute for Neurosciences UMR 5297,
Universite de Bordeaux,
146 rue Leo Saignat,
Bordeaux 33077, France
E-mail: laurent.groc@u-bordeaux2.fr

Autoimmune synaptic encephalitides are recently described human brain diseases leading to psychiatric and neurological syndromes through inappropriate brain–autoantibody interactions. The most frequent synaptic autoimmune encephalitis is associated with autoantibodies against extracellular domains of the glutamatergic *N*-methyl-D-aspartate receptor, with patients developing psychotic and neurological symptoms in an autoantibody titre-dependent manner. Although *N*-methyl-D-aspartate receptors are the primary target of these antibodies, the cellular and molecular pathway(s) that rapidly lead to *N*-methyl-D-aspartate receptor dysfunction remain poorly understood. In this report, we used a unique combination of high-resolution nanoparticle and bulk live imaging approaches to demonstrate that anti-*N*-methyl-D-aspartate receptor autoantibodies from patients with encephalitis strongly alter, in a time-dependent manner, the surface content and trafficking of GluN2-NMDA receptor subtypes. Autoantibodies laterally displaced surface GluN2A-NMDA receptors out of synapses and completely blocked synaptic plasticity. This loss of extrasynaptic and synaptic *N*-methyl-D-aspartate receptor is prevented both *in vitro* and *in vivo*, by the activation of EPHB2 receptors. Indeed, the anti-*N*-methyl-D-aspartate receptor autoantibodies weaken the interaction between the extracellular domains of the *N*-methyl-D-aspartate and Ephrin-B2 receptors. Together, we demonstrate that the anti-*N*-methyl-D-aspartate receptor autoantibodies from patients with encephalitis alter the dynamic retention of synaptic *N*-methyl-D-aspartate receptor through extracellular domain-dependent mechanism(s), shedding new light on the pathology of the neurological and psychiatric disorders observed in these patients and opening possible new therapeutic strategies.

Keywords: glutamate signalling; lateral diffusion; high-resolution nanoparticle imaging

Abbreviations: AMPAR = alpha-amino-3-hydroxy-5-methyl-4-isoxazolepropionic acid receptor; EPHB2R = Ephrin-B2 receptor; GABA = γ-aminobutyric acid; IgG = immunoglobulin G; NMDA = *N*-methyl-D-aspartate; SEP = super-ecliptic pHluorin

Received November 29, 2011. Revised January 14, 2012. Accepted February 14, 2012

Introduction

Autoimmune synaptic encephalitides are recently described human brain diseases leading to neurological and psychiatric syndromes through inappropriate brain–autoantibody interactions (Moscato *et al*., 2010; Vincent *et al*., 2010; Lancaster *et al*., 2011*a*). The worldwide description of these disorders has stimulated fruitful clinical and fundamental investigations, revealing multiple synaptic targets such as the *N*-methyl-D-aspartate (NMDA) receptor (Dalmau *et al*., 2007), the glutamate receptor GluA1 and GluA2 subunits of the alpha-amino-3-hydroxy-5-methyl-4-isoxazolepropionic acid receptor (AMPAR) (Lai *et al*., 2009), the leucine-rich glioma-inactivated 1 protein (Lgi1) (Irani *et al*., 2010; Lai *et al*., 2010), the contactin-associated protein-like 2 (CASPR2) (Irani *et al*., 2010; Lai *et al*., 2010), the glycine receptor (Mas *et al*., 2011), the B1 subunit of the γ-aminobutyric acid-B receptor ($GABA_BR$) (Lancaster *et al*., 2010) or the metabotropic glutamate receptor 5 (Lancaster *et al*., 2011*b*). Among all of these targets, the most frequent synaptic autoimmune encephalitis is associated with autoantibodies against the NMDA receptor (Dalmau *et al*., 2007, 2008, 2011; Chapman and Vause, 2011). Classically, patients first present psychiatric symptoms with paranoid and delusional thinking, perceptual disturbances, agitation, changes in speech, and bizarre behaviour and are possibly misdiagnosed with an acute psychotic break or drug abuse (Dalmau *et al*., 2011). A few days later, patients deteriorate neurologically, with symptoms such as seizures, dyskinesia, altered levels of consciousness and autonomic and breathing instability. Despite the severity of neuropsychiatric symptoms, ~80% of patients fully recover after immunomodulatory treatments such as intravenous immunoglobulins, corticosteroids, cyclophosphamide or rituximab (Dalmau *et al*., 2011). Some cognitive symptoms (disinhibition, poor attention, impulsivity) often persist several months after the acute phase of illness. Importantly, circulating NMDA receptor autoantibodies observed in the CSF and serum of these patients seem to play a direct role in the neurological syndromes. Indeed, a good clinical outcome is fully correlated with a significant decrease of NMDA receptor autoantibodies in patients' CSF (Dalmau *et al*., 2008, 2011). The NMDA receptor autoantibodies decrease NMDA receptor cluster density in a manner that is reversible with the removal of the antibodies from neuronal cell cultures (Dalmau *et al*., 2008; Hughes *et al*., 2010). This effect is independent of the presence of complement, spares other synaptic proteins and does not affect excitatory synaptic density (Dalmau *et al*., 2008; Hughes *et al*., 2010). Furthermore, patients' CSF and purified immunoglobulins type G (IgGs) impaired glutamatergic transmission *in vivo* (Manto *et al*., 2010). Thus, the anti-NMDA receptor autoantibodies present in patients with encephalitis could specifically act on surface NMDA receptors, in a reversible manner since immunotherapy leads to rapid recovery from neurological symptoms (Lee *et al*., 2009; Dalmau *et al*., 2011).

In this study, we took advantage of the identification and purification of these newly identified autoantibodies to acutely explore the cellular pathways activated during these neurological symptoms. The NMDA receptor autoantibodies are IgGs directed against extracellular epitopes of the GluN1 subunit (Dalmau *et al*., 2008, 2011). NMDA receptors are ionotropic glutamate receptors, structured as heteromeric channels comprising various combinations of GluN1, GluN2 and GluN3 subunits, which confer specific biophysical and pharmacological properties (Cull-Candy and Leszkiewicz, 2004). In hippocampus or cortex, the most abundant NMDA receptors are composed of GluN1 subunits associated with GluN2A (enriched in synapses) and/or GluN2B subunits (Wenthold *et al*., 2003). NMDA receptors are trafficked to and from the plasma membrane through exocytosis and endocytosis, respectively (Petralia *et al*., 2003), and their surface distribution and synaptic content is highly dependent on their lateral diffusion (Triller and Choquet, 2005). Recently, NMDA receptor synaptic content has been shown to be regulated by the expression level of the receptor tyrosine kinase EPHB2 (EPHB2R) and EPHB2R activation was shown to impact on NMDA receptor trafficking and synaptic targeting (Henderson *et al*., 2001; Nolt *et al*., 2011). EPHB2R directly associates with the NMDA receptor through the extracellular region of the GluN1 subunit (Dalva *et al*., 2000) and this interaction plays an important role in regulating synaptic function.

To explore the dynamics of NMDA receptor subtypes in the presence of the autoantibodies and to shed light on the NMDA receptor-dependent synaptic regulation (Hughes *et al*., 2010), we used a combination of high-resolution single particle and bulk imaging approaches in hippocampal neurons. Our data revealed that the presence of autoantibodies against NMDA receptors differentially alters the surface trafficking and distribution of GluN2-NMDA receptor subtypes, both in synapses and in extrasynaptic areas. The data further indicate that the interaction between NMDA receptors and EPHB2R is prevented by NMDA receptor antoantibodies and rescued by ephrin-B2 activation of EPHB2R. Identifying, at the single molecule level, the dysfunction of GluN2-NMDA receptor surface trafficking in a model of encephalitis clearly opens possibilities for new therapeutic strategies in broader neurological disorders involving NMDA receptor dysfunction.

Materials and methods

Patient cerebrospinal fluid and purified immunoglobulin G

CSF was obtained from different patients with typical encephalitis with antibodies to GluN1/GluN2 heteromers of the NMDA receptor (Table 1) (Dalmau *et al*., 2008). In both cases, the CSF or serum were collected at symptom presentation, before any treatment and stored at −80°C at NeuroBioTec (Biobank of the Hospices Civils de Lyon, France). The presence of anti-glutamate receptor NMDA receptor1 (NR1) antibodies was demonstrated as reported previously (Dalmau *et al*., 2007). For control CSF and IgG, we selected a patient with an autoimmune disorder, paraneoplastic sensory neuronopathy (anti-Hu autoantibodies), and a patient without an autoimmune disorder but with dementia and brain tumour (Table 1). IgGs were purified (concentration 2 mg/ml) as previously described (Manto *et al*., 2007) from the serum of different patients with encephalitis and NMDA receptor autoantibodies (Table 1). All samples were dialyzed against phosphate-buffered saline and solutions were used at pH 7.4.

Table 1 Clinical features of the patients and controls used in the study

Patient ID	Age/sex	Symptoms	Cancer	Outcome
09-049[a] (CSF)	4/M	Seizures, psychiatric symptoms, orofacial dyskinesia	No	Total recovery
09-030 (CSF)	11/F	Psychiatric symptoms, abnormal movements, seizures, dysautonomia	No	Psychiatric symptoms
09-052 (IgGs[b])	24/F	Seizures, psychiatric symptoms, orofacial dyskinesias, severe dysautonomia	Ovary teratoma	No improvement; death
09-343 (IgGs[b])	24/M	Psychiatric symptoms, abnormal movements, seizures, dysautonomia	No	Total recovery
09-667 (IgGs[b])	22/F	Psychiatric symptoms, orofacial dyskinesia, seizures, dysautonomia	No	Total recovery
09-630 (IgGs[b])	22/F	Psychiatric symptoms, orofacial dyskinesia, seizures	No	Psychiatric symptoms
09-007 (IgGs[b])	32/F	Psychiatric symptoms, seizures, dysautonomia	Ovary teratoma	Total recovery
Controls				
SNP 793 (CSF; IgGs[b])	58/M	Sensory neuronopathy with anti-Hu antibodies	Small cell lung carcinoma	Stable
10-450 (IgGs[b])	68/F	Dementia	Brain tumour	Death

a Described in Lebas *et al*. (2010).
b IgGs purified from patient sera.

Cell culture, immunocytochemistry, synaptic live staining and protein expression

Cultures of hippocampal neurons were prepared from embryonic Day 18 Sprague–Dawley rats. Cells were plated at a density of 50×10^3 cells per ml on polylysine precoated cover-slips. Cover-slips were maintained in a 3% horse serum containing neurobasal medium. This medium was replaced after 4 days *in vitro* by a serum-free neurobasal medium. Cultures were maintained at 37°C in 5% CO_2 for a maximum of 20 days *in vitro*. For immunostaining, surface endogenous GluN1 and EPHB2R were specifically stained in live neurons using polyclonal antibodies against GluN1 (1/300, Alomone labs, 15 min, 37°C) and EPHB2R (R&D systems, 1/200, 15 min, 37°C). Patient and control IgG were incubated for 2 h on live neurons at 37°C in culture medium. Neurons were then fixed with 4% paraformaldehyde for 15 min. To label postsynaptic areas, neurons were permeabilized using 0.1% Triton X-100, incubated with primary polyclonal antibodies against Shank (gift from Gundelfinger, 1/750, 45 min). Finally, neurons were incubated with secondary antibody anti-rabbit Alexa 568 antibodies (Invitrogen, 1/500, 45 min), anti-human Alexa 488 antibodies (Invitrogen, 1/500, 45 min) or anti-goat Alexa 488 antibodies (Invitrogen, 1/500, 45 min). Neurons were washed, mounted and preparations were kept at 4°C until observation. For live imaging, neurons were transfected at 7–14 days *in vitro* using the Effecten transfection kit (QIAGEN) according to the manufacturer's protocol.

Single particle tracking and surface diffusion calculation

Single particle (quantum dot) labelling and microscopy was performed as previously described (Groc *et al*., 2007*b*). Briefly, hippocampal primary neurons were incubated for 10 min (37°C) with polyclonal antibodies against GluN2A subunit (Alomone Labs, 1/500), GluN2B subunit (Alomone Labs, 1/500), EPHB2R (R&D systems, 1/500), GFP (Invitrogen, 1/10 000); and monoclonal antibodies against α2 $GABA_A$ subunit (gift A. Triller, 1/5000), Kv1.3 (Alomone Labs, 1/2000), haemagglutinin (HA)-tag (Roche, 1/1000) and patients' IgG. Neurons were then washed and incubated for 10 min (37°C) with quantum dots 655 goat $F(ab')_2$ anti-rabbit, rabbit $F(ab')_2$ anti-goat IgG, 655 goat $F(ab')_2$ anti-mouse IgG and 655 rabbit $F(ab')_2$ anti-human IgG (for coupling with patient's IgG) (Invitrogen, 1/1000). Non-specific binding was blocked by the addition of casein (Vector Laboratories) to the quantum dots 15 min before use. For single particle tracking of D1 and GluA1 receptor, hippocampal primary neurons were transfected by either D1-CFP or GluA1-HA and Homer1c-GPF as a synaptic marker. For single particle tracking of GluN2A, GluN2B, α2 GABAA and EPHB2 receptors, Kv1.3 channel green MitoTracker® (Invitrogen, 1-min incubation, 20 nM) was used as a synaptic marker. Quantum dots were detected by using a mercury lamp and appropriate excitation/emission filters. Images were obtained with an acquisition time of 50 ms with up to 1000 consecutive frames. Signals were detected using an EM-CCD camera (Quantem, Roper Scientific). Quantum dots were followed on randomly selected dendritic regions for up to 20 min. Quantum dot recording sessions were processed with the MetaMorph® software (Universal Imaging Corp.). The instantaneous diffusion coefficient, D, was calculated for each trajectory, from linear fits of the first four points of the mean-square-displacement versus time function using $MSD(t) = <r^2>(t) = 4Dt$. The 2D trajectories of single molecules in the plane of focus were constructed by correlation analysis between consecutive images using a Vogel algorithm.

Fluorescent recovery after photobleaching

Neurons co-transfected with Homer1c-DsRed and either super-ecliptic pHluorin (SEP) labelled subunits GluN2A-SEP, GluN2B-SEP or GluN1-SEP were placed on the heated stage (37°C) of an inverted confocal spinning-disk microscope (Leica). To test the population of surface GluN subunits-SEP, we used low pH-solution adjusted to pH 5.4 which quenched all the fluorescence indicating that SEP allows the specific visualization of surface receptors (Bard *et al*., 2010).

Fluorescence was excited using a monochromator controlled by MetaMorph® software (Universal Imaging). To photobleach locally, we used a Sapphire laser 488-20 at 50% power to avoid photo damage. The laser was coupled to the microscope via galvanometric mirrors, which allowed us to photobleach several regions within a short time window. Recovery from photobleach was monitored by two consecutive acquisition periods at 2 and 0.5 Hz acquisition rate, respectively. Recovery curves were corrected for continuous photobleaching and background noise. For the follow-up of cluster fluorescence intensity to assess synaptic receptor content, neurons were co-transfected with Homer1c-DsRed, GluN2A-SEP and GluN2B-SEP. Clusters were imaged over a period of 30 min after a chemically induced potentiation protocol (chemical long-term potentiation), as previously described (Lu *et al*., 2001; Park *et al*., 2004, 2006; Wang *et al*., 2008), glycine (200 μM) and picrotoxine (5 μM) were applied for 4 min. Bath co-application of glycine and picrotoxin was always applied after the recording of the basal condition in live experiments and the medium was carefully replaced by new equilibrated and heated medium after the protocol application. Fluorescence intensity was measured using MetaMorph® software (Universal imaging) and corrected for photobleaching and background noise.

In vivo injection and immunohistochemistry

Adult female FVB mice were anaesthetized by isoflurane and stereotaxic surgery was performed. Ejection pipettes were lowered into the dorsal hippocampus at the following coordinates: −2.2 mm from bregma, 1.5 mm from midline, 1.5 mm from brain surface. Purified patient IgG alone (400 nl, 1 mg/ml), purified control IgG alone (400 nl, 1 mg/ml), 200 nl of purified patient IgG (2 mg/ml) mixed with 200 nl ephrin-B2 ligand (50 μg/ml) or 200 nl of purified control IgG (2 mg/ml) mixed with 200 nl ephrin-B2 ligand (50 μg/ml) was injected into the dorsal hippocampus (2 × 200 nl with 200 μm separation distance). For each mouse, two different solutions (purified patient IgGs and ephrin-B2 ligand or purified control IgG and ephrin-B2 ligand) were injected in either the right or left hemisphere. Mice were recovered and perfused 5–7 h after injection with 4% paraformaldehyde (pentobarbital anaesthesia). Brains were removed and bathed in 4% paraformaldehyde (2 h), incubated overnight in 15% sucrose (4°C) and then snap-frozen in isopentane. Coronal sections of the brain (12 μm) were obtained on a microtome (Leica). For immunohistochemistry, after 1 h incubation with 2% normal goat serum in phosphate-buffered saline at room temperature, coronal sections of the brain were incubated with polyclonal antibodies against GluN2A subunit (Alomone Labs, 1/100) or monoclonal antibodies against GluN1 subunit (Millipore, 1/500) overnight at room temperature. Fluorescent revelation was carried out with fluorophore-labelled secondary antibodies anti-mouse Alexa568 (Invitrogen, 1/400) or anti-rabbit Alexa488 (Invitrogen, 1/400) for 2 h at room temperature. Images were obtained using a confocal microscope (SP2, Leica) and processed for analysis. Using MetaMorph software (Universal imaging), a threshold was applied on each image in order to extract cluster staining and the cluster fluorescence was measured.

Calcium imaging

Hippocampal neurons (14–18 days *in vitro*) were incubated with a fluorescent calcium indicator Fluo-4, AM FluoroPure™ grade (Invitrogen, 2 μM, 10 min, 37°C) in artificial CSF (NaCl 140 mM, KCl 5 mM, $CaCl_2$ 2.5 mM, MgCl2 1.6 mM, HEPES 10 mM, D-glucose 24 mM, Sigma Aldrich). Neurons were then washed and placed on the heated stage (37°C) of an inverted confocal spinning-disk microscope (Leica) and imaged over a period of 30 min (acquisition rate 0.02 Hz) after glutamate (30 μM, Sigma Aldrich) stimulation in the presence of an AMPAR antagonist [2,3-dihydroxy-6-nitro-7-sulphamoyl-benzo[f]quinoxaline-2,3-dione (NBQX), 20 μM, Tocris], Na-channel blocker [tetrodotoxin (TTX), 1 μM, Tocris] and L-type calcium channel blocker (nifedipine, 5 μM, Tocris). Glutamate stimulation was always applied after the recording of the basal condition. In control conditions, a transient calcium increase was blocked by the NMDA receptor antagonist [2-amino-5-phosphonopentanoic acid (AP-5), 10 μM, Tocris]. Fluorescence intensity was measured using MetaMorph software (Universal imaging) and corrected for photobleaching and background noise.

Antibody feeding assay

Primary hippocampal neuron cultures were prepared from embryonic C57Bl6 mouse brains (embryonic Day 17) as previously described (Goslin and Banker, 1991). Live hippocampal neurons (14–17 days *in vitro*) were incubated for 20 min at 37°C with an antibody directed against the extracellular region of the NMDA receptor subunit GluN1 (R1JHL, Calbiochem). After washing in phosphate-buffered saline, neurons were treated in neurobasal medium with patient or control IgG with or without clustered ephrin-B2-Fc for 20 h at 37°C. Then, neurons were fixed for 4 min at room temperature in 4% paraformaldehyde/4% sucrose. Pre-labelled surface receptors were stained, without permeabilization, using a saturating amount of Alexa 488-conjugated secondary antibody (Invitrogen) overnight at 4°C. Neurons were subsequently permeabilized at room temperature for 30 min with a phosphate-buffered saline/bovine serum albumin/0.3% Triton X-100 solution, and pre-labelled internalized receptors were stained with a biotinylated-conjugated secondary antibody followed by streptavidin-Alexa 647 (Invitrogen) treatment. Then, neurons were incubated with an antibody directed against microtubule-associated protein 2 (MAP2, Millipore), followed by an Alexa 555-conjugated secondary antibody (Invitrogen). Finally neurons were counterstained with DAPI. Fluorescence images were acquired with a Zeiss microscope equipped with epifluorescent illumination and apotome technology. Stained neurons were then blindly analysed using ImageJ software (NIH). Images were first thresholded to assess apical dendrite area. The number of GluN1 subunit clusters was assessed in each region of interest and divided by the region of interest area. Receptor clusters were ∼0.2–0.6 μm in length. To calculate the proportion of surface NMDA receptors that were maintained at the cell surface, the density of surface GluN1 subunit clusters was divided by the total (surface + intracellular) density of GluN1 subunit. All values were normalized to those of neurons treated with control IgG. Each condition was performed on six coverslips and was expressed as mean ± SEM.

Co-immunoprecipitation and western blot

Cultured hippocampal neurons (15 days *in vitro*) were incubated with IgGs from Patient 09-343 (25 μg/ml) and Control SNP793 (25 μg/ml) for 5 h at 37°C. Cells were then lysed with PathScan® sandwich ELISA lysis buffer (Cell Signalling Technology, Inc), for 5 min on ice. Lysates were sonicated and spun at 8000 *g* for 15 min at 4°C. Supernatants were quantified, aliquoted and stored at −80°C. EPHB2R (goat polyclonal antibody, 12 g, R&D systems) antibody was incubated under

constant agitation at 37°C overnight with 20 µl of tosyl-activated-magnetic beads (Dynabeads M-280 tosylactivated, Invitrogen), which were washed twice with coupling buffer A (0.1 M borate buffer pH 9.5) and supplemented with coupling buffer C (3 M ammonium sulphate in buffer A) beforehand. The antibody-bead mixtures were washed with blocking buffer (phosphate-buffered saline pH 7.4/0.5% bovine serum albumin), 1 h at 37°C under constant agitation and with washing buffer (phospate-buffered saline pH 7.4/0.1% bovine serum albumin). Cell lysates treated with patient and control IgG were added to antibody-bead mixtures and incubated under constant agitation for 4 h at 24°C. Beads were then thoroughly washed four times with PathScan® sandwich ELISA lysis buffer. The beads were resuspended into 40 µl of 2 × sample buffer. Before loading on a gel, the samples were boiled at 100°C for 5 min. Sample supernatants (10 µl, without beads) were separated by sodium dodecyl sulphate-polyacrylamide gel electrophoresis (Mini-Protean TGX precast gels 4–20%, Bio-Rad) for 40 min at 200 V and transferred onto nitrocellulose membrane for 1 h at 100 V. After blocking for 1 h in 5% milk in Tris–saline-0.05% Tween-20 (TBST), the membranes were incubated for 1 h at room temperature with a monoclonal antibody against GluN1 subunit (clone 54.1, BD Pharmingen) or a monoclonal antibody against tubulin (clone TUB 2.1, Sigma), diluted at 1 and 0.2 g/ml, respectively, in TBST 0.5% milk. Secondary antibodies coupled with horseradish peroxidase were used at 1:10 000 in TBST 0.5% milk. Detection was performed using the SuperSignal® West Femto Maximum Sensitivity Substrate detection System (Pierce) revealed with a ChemiGenius system (Syngene). Quantification of band intensity was performed using Genetools software (Syngene).

Data and statistical analysis

The instantaneous diffusion coefficient is reported as the median ± 25–75% (interquartile range, IQR). All of the other group values are expressed as mean ± SEM. Each data series was obtained from 2 to 5 independent experiments (e.g. for each *in vitro* data set: 3–5 independent cell cultures, 6–10 different cover-slips per cell culture). Comparisons between groups were either performed with parametric statistical tests (surface immunostaining) or with non-parametric Mann–Whitney test (single quantum dots). Significance levels were defined as $*P < 0.05$, $**P < 0.01$, $***P < 0.001$.

Results

Patient cerebrospinal fluid rapidly alters the surface trafficking of GluN2-NMDA receptor and prevents glutamate synapse long-term potentiation

In anti-NMDA receptor encephalitis, the epitopes of the autoimmune antibodies are located in the extracellular region of GluN1 subunit (Dalmau *et al*., 2008). Furthermore, incubation of hippocampal neurons, for several consecutive days, with patient IgGs potently decreases the surface content of NMDA receptors (Hughes *et al*., 2010). To better explore the kinetics and the molecular cascade involved in this process, we first investigated, on the short-term range, the impact of anti-NMDA receptor antibodies from patient CSF or purified IgGs (Table 1) on the surface content of the two main hippocampal NMDA receptor subtypes, i.e. the GluN2A- and GluN2B-NMDA receptors (Wenthold *et al*., 2003). In cultured hippocampal neurons, these NMDA receptor subunits are exclusively located in the postsynaptic membrane compartment (Bard *et al*., 2010). Hippocampal neurons were transfected with either the GluN2A or GluN2B subunit tagged with SEP at their extracellular N-termini. SEP is a pH-sensitive variant of enhanced GFP that exhibits bright fluorescence when exposed to the exterior of the cell, but has relatively little fluorescence while in internal acidified trafficking organelles (Ashby *et al*., 2004) (Fig. 1A). This allows us to track over time the surface content of NMDA receptors in live hippocampal neurons. Under basal conditions, both GluN2A- and GluN2B-NMDA receptors were detected at the neuronal surface with a clear enrichment of GluN2A-NMDA receptors in postsynaptic density of glutamatergic synapses (detected by the presence of the postsynaptic protein Homer 1c-DsRed) (Supplementary Fig. 1) when compared with GluN2B-NMDA receptors, which are mostly extrasynaptic (Tovar and Westbrook, 1999; Groc *et al*., 2006) (Fig. 1B). Patient CSF incubation (20 h, dilution 1/300) significantly decreased the surface content of GluN2A- and GluN2B-NMDA receptors (Fig. 1B–D), consistent with the already described GluN1-NMDA receptor content decrease after 1–7 days incubation with patient CSF (Dalmau *et al*., 2008; Hughes *et al*., 2010). Interestingly, this effect was time-dependent since after 2 h of incubation the surface content of GluN2B-NMDA receptors was already significantly reduced by 19% (Fig. 1C). Importantly, these major changes in NMDA receptor content were not due to massive loss in synaptic contacts since the overall number of glutamatergic synapses, i.e. the number of Homer clusters, remained unaffected by patient CSF incubation (up to 24 h) (Supplementary Fig. 2).

Since synaptic NMDA receptors play a key role in synaptic plasticity processes (Yashiro and Philpot, 2008) that serve as cellular substrates for learning and memory (Morris, 2006), we explored the functional impact of patient CSF on synaptic long-term potentiation (chemical long-term potentiation; Lu *et al*., 2001, 2007; Wang *et al*., 2008). Based on the massive reduction of surface and synaptic NMDA receptors one would predict that the induction of synaptic long-term potentiation is altered in neurons exposed to patient CSF. To test this, the synaptic content of the glutamatergic AMPAR containing the GluA1 subunits was measured using GluA1-SEP expression in hippocampal neurons (Fig. 1E). In neurons incubated with the control CSF (20 h, dilution 1/300), the synaptic content of GluA1-AMPAR was significantly increased following the induction of chemical long-term potentiation (Fig. 1E–G). However, in neurons exposed to patient CSF (20 h, dilution 1/300) the long-term potentiation protocol failed to increase the synaptic content of surface AMPAR from the basal level (Fig. 1E–G), indicating that patient CSF drastically reduces the plastic range of glutamate synapses. It should be noted that a shorter incubation (tens of minutes range) of hippocampal neurons with patients' autoantibodies already reduces the extent of long-term potentiation of excitatory currents in the CA1 area (Zhang *et al*., 2012). Together, these data reveal that patient CSF, containing the anti-NMDA receptor antibodies, rapidly reduced GluN2A- (synaptic) and GluN2B- (extrasynaptic) NMDA receptor surface content and reduced potentiation of

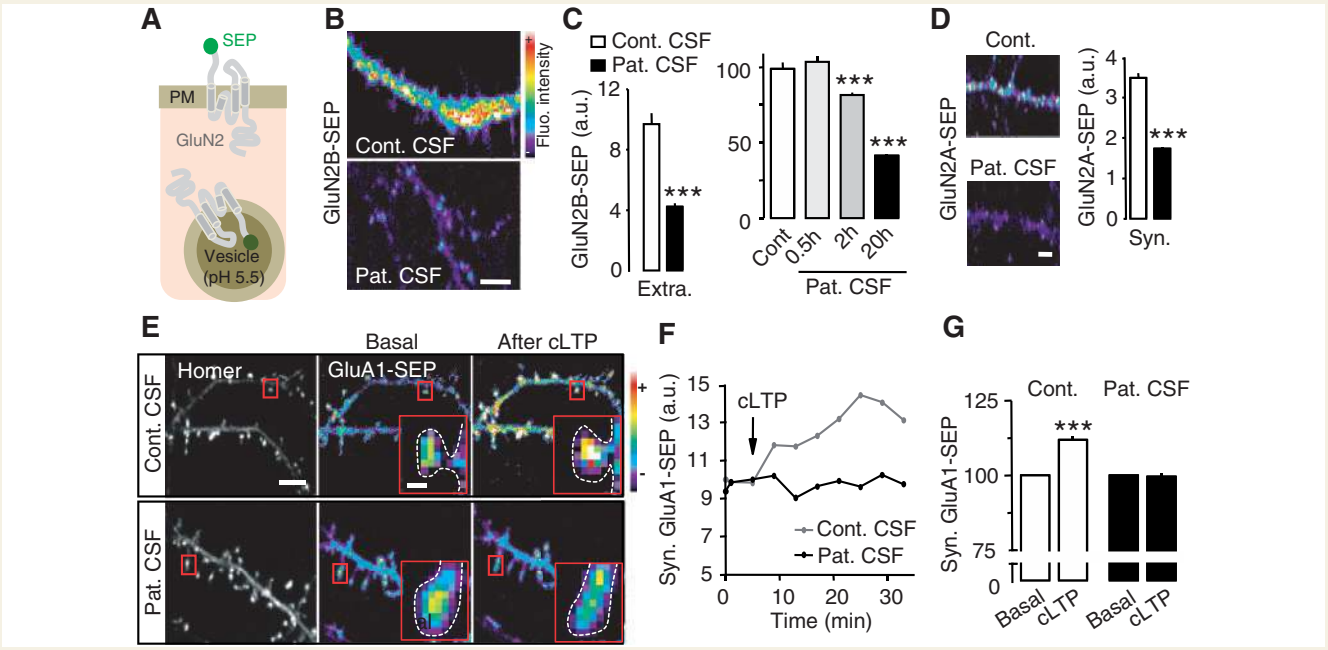

Figure 1 Patient CSF decreases the surface content of both GluN2A- and GluN2B-NMDA receptor in a time-dependent manner and prevents long-term potentiation (LTP) of glutamate synapses. (**A**) Schematic representation of GluN subunit tagged with SEP protein at its N-terminus (extracellular). SEP is quenched at acidic pH (e.g. cycling vesicles) and only emits fluorescence in dendrites when inserted at the plasma membrane. (**B**) GluN2B-SEP dendritic fragments from neurons incubated 20 h either with control (Control SNP 793 CSF; dilution 1/300) or patient CSF (Patient 09-049 CSF; dilution 1/300). Scale bar = 5 μm. (**C**) Fluorescence intensity of GluN2B-SEP was significantly decreased by patient CSF in the extrasynaptic compartments (*left*) (control CSF: $n = 100$ clusters; patient CSF: $n = 60$, 20-h incubation). Moreover, patient CSF decreased, in a time dependent manner (0.5, 2 or 20 h), the global fluorescence intensity of GluN2B-SEP with a significant decrease already observed at 2 h (*right*). Data from each time point was compared to its own control value (control $n = 278$ clusters; patient CSF 0.5 h: $n = 40$; patient CSF 2 h: $n = 50$, patient CSF 20 h: $n = 217$). (**D**) GluN2A-SEP dendritic fragments from neurons incubated for 20 h either with control (Control SNP 793 CSF; dilution 1/300) or patient CSF (Patient 09-049 CSF; dilution 1/300). Scale bar = 5 μm. The fluorescence intensity of GluN2A-SEP was significantly decreased by patient CSF in the synaptic compartment (control CSF: $n = 115$ clusters; patient CSF: $n = 104$). (**E**) Representative dendritic fragments of hippocampal neurons expressing Homer 1c-DsRed and AMPAR (GluA1-SEP) before (basal) and after chemical long-term potentiation (cLTP) protocol. The pseudocolour GluA1-SEP subunit representation shows the different intensity levels of the GluA1-SEP staining. Note that after chemical long-term potentiation the GluA1-SEP fluorescence (colour-coded) increased in postsynaptic areas. In neurons incubated with control CSF (Control SNP 793 CSF) the relative GluA1-SEP fluorescence increased after chemical long-term potentiation whereas in the presence of Patient 09-030 CSF (20 h; 1/300) the relative GluA1-SEP fluorescence remains stable before and after chemical long-term potentiation (*lower* panels). Scale bars: main panels = 6 μm; insets = 300 nm. (**F**) Representative quantification of GluA1-SEP synaptic clusters (at least 30 min) in the presence of control (grey line) or patient (black line) CSF. The induction of chemical long-term potentiation after a 5-min baseline period increased GluA1-SEP synaptic fluorescence (arbitrary unit, a.u.) in control but not in patient CSF. (**G**) Relative synaptic GluA1-SEP intensity before and after chemical long-term potentiation in control ($n = 211$ synapses) and patient CSF conditions ($n = 315$ synapses). Note the significant increase to 112% of basal condition in control CSF after chemical long-term potentiation. $***P < 0.001$.

glutamatergic synapses, further suggesting that patient anti-NMDA receptor antibodies affect the trafficking of surface NMDA receptor.

Patient immunoglobulin Gs differentially affect synaptic (GluN2A) and extrasynaptic (GluN2B) NMDA receptor surface diffusion

Over the last decade it has emerged that the surface distribution of NMDA receptors highly depends on their diffusion in the plasma membrane (Bard and Groc, 2011). To identify the cellular pathway(s) by which patient anti-NMDA receptor antibodies control the surface content of GluN2-NMDA receptor, we explored the possibility that patient CSF primarily affects the surface dynamics of NMDA receptors. For this, we used two complementary approaches. First, we expressed GluN2A-SEP and GluN2B-SEP in hippocampal neurons and investigated the impact of patient CSF on the surface diffusion using the fluorescence recovery after photobleaching (FRAP) approach (Lippincott-Schwartz and Patterson, 2003) (Fig. 2A). Strikingly, the fraction of mobile surface GluN2A- and GluN2B-NMDA receptor, measured by the amount of fluorescence recovery (Fig. 2B, C), was differentially affected by patient CSF (20 h, dilution of 1/300). Indeed, patient CSF significantly increased the mobile fraction of GluN2A-NMDA receptor and significantly decreased the mobile fraction of GluN2B-NMDA receptor (Fig. 1C), suggesting that

synaptic GluN2A-NMDA receptor was mostly removed from synapses whereas extrasynaptic GluN2B-NMDA receptors were mostly cross-linked.

To directly investigate the impact of patient anti-NMDA receptor antibodies at the single receptor level, we used the single nanoparticle (quantum dot) approach that isolates single particle-receptor complexes with a sub-wavelength precision (Groc *et al*., 2007*b*; Triller and Choquet, 2008) (Fig. 2D). First, purified IgGs containing anti-NMDA receptor antibodies were isolated from patients and used to further identify the nature of their membrane target. Consistent with previous observations (Dalmau *et al*., 2007; Hughes *et al*., 2010), the surface labelling of the patient IgGs was similar to the one against the surface GluN1 subunit, which was concentrated in synaptic areas (Supplementary Fig. 3). Then, to measure in live neurons the membrane dynamics of the IgGs' target and investigate the possible acute (minute range) effect of the IgGs, we coupled patient IgG to single quantum dots, incubated neurons for ~10 min and tracked the complexes over time (Supplementary Fig. 4A). Globally, two main surface behaviours were observed, i.e. a high diffusion pattern that explored a large dendritic area and a low diffusion pattern that was highly confined (Supplementary Fig. 4A). When the diffusive trajectories crossed glutamatergic synapses they were only transiently retained (Supplementary Fig. 4B), whereas the slowly diffusing trajectories were highly retained in such synapses. When we compared, in the same neuronal preparation, the diffusion characteristics (per cent of immobile receptors that are defined as: diffusion coefficient $< 0.005\,\mu m^2/s$) of surface GluN2A- and GluN2B-NMDA receptor, GluA2-AMPAR, α2-GABA$_A$R and EPHB2R, it clearly emerged that patient IgGs quantum dot trajectories displayed a comparable immobile receptor fraction with GluN2A- and GluN2B-NMDA receptors (Supplementary Fig. 4C). This result suggests that patient anti-NMDA receptor IgGs initially target surface NMDA receptors without inducing, at least in the tens of minute time range used in this experiment, a major effect on their surface diffusion.

We then measured the effects of IgGs on hippocampal neurons incubated for at least 2 h with purified IgGs from anti-NMDA receptor patients (Patient IgG: 50 μg/ml) or control patients (Control IgG: 2 h, 50 μg/ml). After incubation, single GluN2A- or GluN2B-NMDA receptor quantum dot complexes were tracked at the surface of neurons. The imaging sessions were done blindly, not knowing control versus patient conditions. Surface GluN2A-NMDA receptor that are confined and anchored in synapses under the control IgG condition became highly diffusive and accumulated in the extrasynaptic compartment under the patient IgG condition (Fig. 2D and E). In contrast, surface GluN2B-NMDA receptors that are rather diffusive under the control IgG condition became highly confined under the patient IgG condition (Fig. 2D and E). Thus, consistent with the fluorescence recovery after photobleaching data, the surface confinement of GluN2B-NMDA receptor likely results from an IgG-induced cross-linking of the surface receptors (Groc *et al*., 2008; Heine *et al*., 2008; Hughes *et al*., 2010) whereas the lateral escape of GluN2A-NMDA receptors outside the synapse revealed the presence of a critical retention mechanism that is prevented by the binding of patient IgGs on extracellular domain(s) of NMDA receptors (Dalmau *et al*., 2008). In order to compare the cellular effect of IgGs from different patients and controls, we blindly measured the impact of IgGs from five different patients with anti-NMDA receptor antibodies and two different control patients (Table 1) on the surface diffusion of the synaptic GluN2A-NMDA receptors, since these receptors were rapidly displaced from synapses by the presence of the patient IgGs. As shown in Fig. 2F, IgGs from each patient similarly displaced GluN2A-NMDA receptors out of synapses within a 2-h incubation period whereas the two control IgGs had no effect (Fig. 2F), indicative of an all-or-none effect. In addition, this effect was dose-dependent since high dilutions of patient IgGs (Patient 09-030, Table 1) reduced the effect (Fig. 2G). Finally, it should be noted that we previously demonstrated that the presence of 'control' IgG (e.g. anti-rabbit IgG) does not affect the surface diffusion of glutamate receptors, measured by single nanoparticle/molecule tracking and fluorescence recovery after photobleaching approaches (Groc *et al*., 2007*b*, 2008; Heine *et al*., 2008). Together, these data demonstrate that IgGs from different patients with anti-NMDA receptor antibodies interfere with the same potency and in a dose-dependent manner with the synaptic retention of GluN2A-NMDA receptors, suggesting that IgGs of patients with NMDA receptor encephalitis prevent a molecular interaction and/or cellular pathway that anchors GluN2A-NMDA receptor in the postsynaptic area.

The interaction between surface GluN2A-NMDA receptors and EPHB2R is disrupted by patient immunoglobulin Gs

To uncover this molecular pathway we first investigated the impact of patient IgGs on the trafficking of other surface neurotransmitter receptors and ion channels that are present in the same neurons and surface compartments. In presence of patient IgGs (2–3 h), we measured the lateral diffusion of the surface GluA1-AMPAR, the metabotropic dopamine D1 receptor, the α2-GABA$_A$R and potassium ion channel Kv1.3 D1 receptor surface diffusion was not affected by patient IgGs (Fig. 3A and B). The GluA1-AMPAR diffusion was slightly increased although to a much lower extent than for GluN2-NMDA receptor (Fig. 3A and B). The diffusion of the α2-GABA$_A$R, which laterally explores both inhibitory and excitatory synapses (Bannai *et al*., 2009), was not affected by patient IgGs. Finally, the surface diffusion of the potassium channel Kv1.3, which is present all over the dendritic tree and binds to the same PDZ domain-containing scaffold proteins as the NMDA receptors (Lim *et al*., 2002), was unaffected by patient IgGs (Fig. 3A and B). Taken together, these data indicate that patient IgGs do not have major influence on the surface dynamics of other receptors and ion channels, suggesting a rather specific action on GluN2-NMDA receptor trafficking.

The intracellular domain of the GluN subunits of NMDA receptors interact with numerous partners (Wenthold *et al*., 2003). However, only few direct partners of the extracellular domain of GluN subunits have been identified. Among these, the EPHB2R (Dalva *et al*., 2000) binds ephrin-B2 ligand in the synapses and

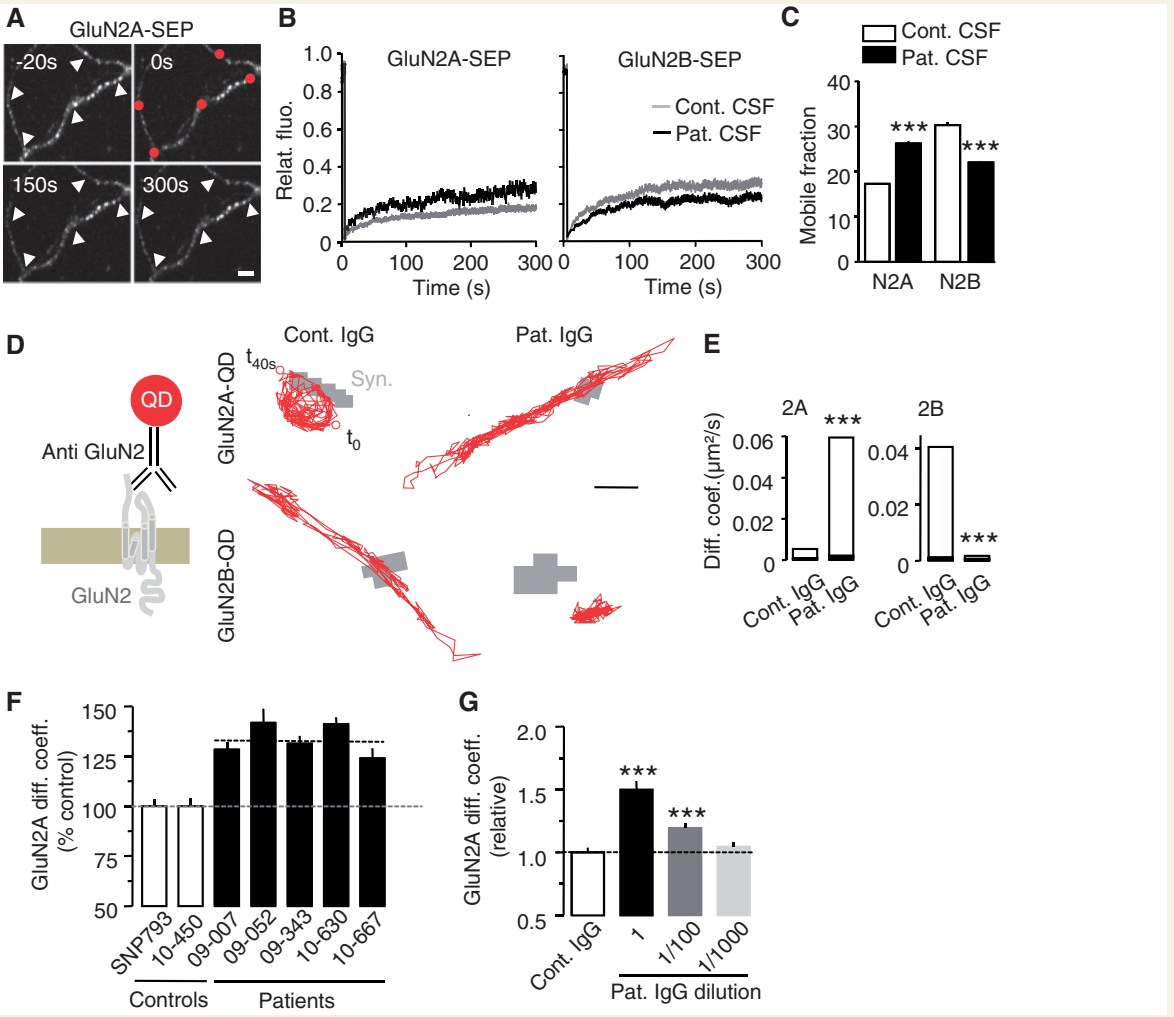

Figure 2 Patient IgG differentially affects the surface diffusion of GluN2A- and GluN2B-NMDA receptors. (**A**) Representative acquisition of fluorescence recovery after photobleaching (FRAP) of GluN2A-SEP in control CSF. Some GluN2A-SEP clusters were photobleached (red circles) and the fluorescence recovery was followed over time (up to 300 s). Scale bar = 5 μm. (**B**) Expression of GluN2A- (*left*) and GluN2B- (*right*) SEP fluorescence recovery versus time after control (grey line; Control SNP 793 CSF; 20 h, 1/300) or patient (Patient 09-030 CSF; black line; 20 h, 1/300) CSF incubation. (**C**) The mobile fraction was significantly increased for GluN2A-SEP (control $n = 68$ photobleached clusters, $n \geqslant 4$ neurons; patient $n = 24$, $n \geqslant 4$ neurons; $^{***}P < 0.001$) and decreased for GluN2B-SEP (control $n = 55$, $n \geqslant 4$ neurons; patient $n = 73$, $n \geqslant 4$ neurons; $P < 0.001$). (**D**) Schematic representation of the surface labelling of a GluN2 subunit using a single anti-GluN2 antibody quantum dot (QD) complex (*left*). Representative trajectories of surface GluN2A quantum dots and GluN2B quantum dots (*right*, red lines, 1000 frames, 50 ms acquisition) in neurons incubated with either control or patient IgG (2 h, 5 μg/ml). Glutamate synapses correspond to grey areas. Scale bar = 500 nm. (**E**) The instantaneous diffusion coefficient distributions (median ± 25–75% IQR) of GluN2A and GluN2B subunits in control or patient IgGs (control IgG 'SNP 793' 2A: median = 9×10^{-4} μm²/s, 25–75% = 3×10^{-4}–5×10^{-3} μm²/s, $n = 2085$ trajectories; patient IgG '09-052' 2A: median = 2×10^{-3} μm²/s, 25–75% = 6×10^{-4}–5×10^{-2} μm²/s, $n = 1172$; control IgGs 'SNP 793' 2B: median = 1×10^{-3} μm²/s, 25–75% = 3×10^{-4}–4×10^{-2} μm²/s, $n = 1920$; patient IgG '09-052' 2B: median = 6×10^{-4} μm²/s, 25–75% = 3×10^{-4}–2×10^{-3} μm²/s, $n = 1209$). Note the significant and opposite effect of patient IgG on the GluN2 subunit surface diffusion ($P < 0.001$). (**F**) Membrane instantaneous diffusion coefficient of GluN2A subunit was significantly increased in the presence of five different patient IgGs (Patient 09-007: $n = 1284$ trajectories, $P < 0.001$; Patient 09-052: $n = 1937$ trajectories, $P < 0.001$; Patient 09-343: $n = 1266$ trajectories, $P < 0.001$; Patient 10-630: $n = 1824$ trajectories, $P < 0.001$; Patient 10-667: $n = 735$ trajectories, $P < 0.001$) when compared to two control IgG (Control SNP793: $n = 1478$ trajectories; Control 10-450: $n = 1329$ trajectories). Note that the increase of GluN2A diffusion coefficient was similar between the different patient IgGs. All these experiments were performed blindly. (**G**) Membrane instantaneous diffusion coefficient of GluN2A subunit after 2-h incubation with different dilutions of patient IgG [control IgGs SNP793: 5 μg/ml, $n = 1290$ trajectories and patient IgGs, Patient 09-052 at three different concentrations: 5 μg/ml, $n = 571$ trajectories (dilution 1), 50 ng/ml, $n = 1501$ trajectories (dilution 1/100), 5 ng/ml, $n = 1753$ trajectories (dilution 1/1000)].

efficiently clusters NMDA receptors when activated (Dalva *et al*., 2000, 2007). Thus, the possibility emerges that the binding of patient IgGs on extracellular domains of NMDA receptors reduces the association with EPHB2R. In order to test this hypothesis, we first tracked surface EPHB2R using the single quantum dots approach under different IgG conditions. Under the control IgG condition, EPHB2R were highly diffusive and explored a large area of the neuronal surface (Fig. 3C). Interestingly, in the synapse, EPHB2R quantum dot diffusion was significantly increased by patient IgGs (Fig. 3C and D), consistent with a disruption of the interaction between EPHB2R and a membrane interactor. To investigate whether patient IgGs prevent the direct interaction between EPHB2R and NMDA receptors, we co-immunoprecipitated EPHB2R with the obligatory GluN1 subunit of the NMDA receptor in the presence of control or patient IgGs (5 h, 255 μg/ml). Strikingly, patient IgGs reduced the amount of the EPHB2R-NMDA receptor complex when compared with co-immunoprecipitation in the presence of control IgGs (Fig. 3E), indicating that the interaction between EPHB2R and NMDA receptors is indeed disrupted by patient IgGs. In addition, this disruption reduced the size of the membrane EPHB2R clusters, which are mostly synaptic (~70%) (Fig. 3F and G). Together, these data indicate that patient IgGs prevent the surface interaction between EPHB2R and NMDA receptors, leading to a lateral dispersal of synaptic EPHB2R and NMDA receptors.

Activation of EPHB2R prevents the majority of patient immunoglobulin G-induced NMDA receptor surface trafficking changes

In an attempt to prevent the cellular effects of patient IgGs and favour the retention of NMDA receptors in the plasma membrane and in synapses, we took advantage of the fact that the activation of EPHB2R by its ligand, ephrin-B2, increases the clustering of synaptic NMDA receptors (Dalva *et al*., 2000, 2007). To investigate the impact of EPHB2R activation on surface distribution of NMDA receptors, i.e. testing whether the activation of EPHB2R can counteract the patient IgG-induced NMDA receptor surface dispersal, we first incubated neurons with ephrin-B2 (1255 ng/ml for 25 h) and control IgGs. We reported no significant change in GluN2A-NMDA receptor diffusion (Fig. 4A and B). However, in the presence of patient IgGs (2 h), ephrin-B2 prevented the increased surface diffusion and lateral escape of synaptic GluN2A-NMDA receptors (Fig. 4A and B). This effect was specific since the activation of the N-cadherin receptor, which is present in these synapses and acts indirectly on the NMDA receptor signalling (Tai *et al*., 2008), did not affect patient IgG-induced lateral redistribution of synaptic GluN2A-NMDA receptors (Fig. 4A and B). To further test the role of this interaction on the surface receptor dynamics, neurons were incubated with antibodies directed against an extracellular epitope of EPHB2R and surface GluN2A-NMDA receptors were tracked at the neuronal surface. Remarkably, GluN2A-NMDA receptor surface diffusion was greatly increased (Fig. 4A and B) in presence of anti-EPHB2R antibodies, confirming that in live neurons the synaptic retention of GluN2A-NMDA receptors highly relies on an extracellular interaction between EPHB2R and NMDA receptors. Altogether, these data demonstrate that the ephrin-B2-induced activation of EPHB2R rescues the synaptic retention of GluN2A-NMDA receptors in the presence of NMDA receptor autoantibodies, most likely through the maintenance of the extracellular association between EPHB2 and NMDA receptors.

Based on these results, one might predict that the activation of EPHB2R signalling also affects, in conjunction with the surface dynamics, the membrane content of functional NMDA receptors. To test this, we used calcium imaging to estimate the surface content of functional NMDA receptors in hippocampal neurons exposed to control or patient IgGs (2–45 h). Glutamate (305 μM) was applied onto hippocampal neurons, loaded with a calcium indicator (Fluo-4), in the presence of an AMPAR antagonist (NBQX, 20 μM), sodium channel blocker (TTX, 1 μM) and L-type calcium channel blocker (nifedipine, 5 μM). In control conditions, glutamate produced a transient calcium rise that was blocked by the bath application of the NMDA receptor antagonist AP-5 (10 μM) (Fig. 5A and B). The presence of patient IgGs (2 h) significantly decreases the glutamate-induced calcium rise. It should be noted that this decrease of functional endogenous NMDA receptors is consistent with the surface content decrease of overexpressed GluN2A/B-NMDA receptors (Fig. 1). Remarkably, incubation of neurons with patient IgGs and ephrin-B2 ligands (500 ng/ml for 45 min) produced a large calcium influx upon glutamate stimulation that was significantly higher than the patient IgGs alone condition (Fig. 5C). It could be noted that in the control condition ephrin-B2 ligand only tends to increase the glutamate-induced calcium rise (Fig. 5C). Collectively, these data show that the activation of EPHB2R by its ligand prevents the decrease in functional NMDA receptor and favours their surface retention in presence of patient IgGs.

To further determine how EPHB2R activation impacts on the membrane content of NMDA receptors in the presence of patient IgG, we used an assay that allows the staining of both internalized and remaining surface NMDA receptors in hippocampal neurons. We monitored NMDA receptor internalization by immunostaining the obligatory GluN1 subunit in live neurons because it associates with EPHB2R at the cell surface upon ephrin-B2 stimulation (Dalva *et al*., 2000). In control conditions, a significant internalization of NMDA receptors was observed after 20 h of treatment (Control SNP793 IgG) (Fig. 5D). Stimulation with ephrin-B2 ligand Fc, which allows a significant activation of EPHB2Rs, did not change the surface and total GluN1 subunit cluster density when combined with control IgG (Fig. 5E and F). In contrast, treatment with Patient 10-630 IgG significantly decreased the surface GluN1 subunit cluster density compared with control IgG (Fig. 5E), as previously reported (Hughes *et al*., 2010). Noticeably, this internalization process was not reflected by a parallel increase in the internalized GluN1 subunit cluster density (Fig. 5E). Thus, we reported a decrease in the total GluN1 subunit cluster density (Fig. 5F), suggesting that patient IgG depleted cell surface NMDA receptors by enhancing both their internalization and subsequent degradation. Remarkably, activation of EPHB2R in the presence of patient IgG prevented both the decrease in surface and total GluN1 cluster densities when compared with patient

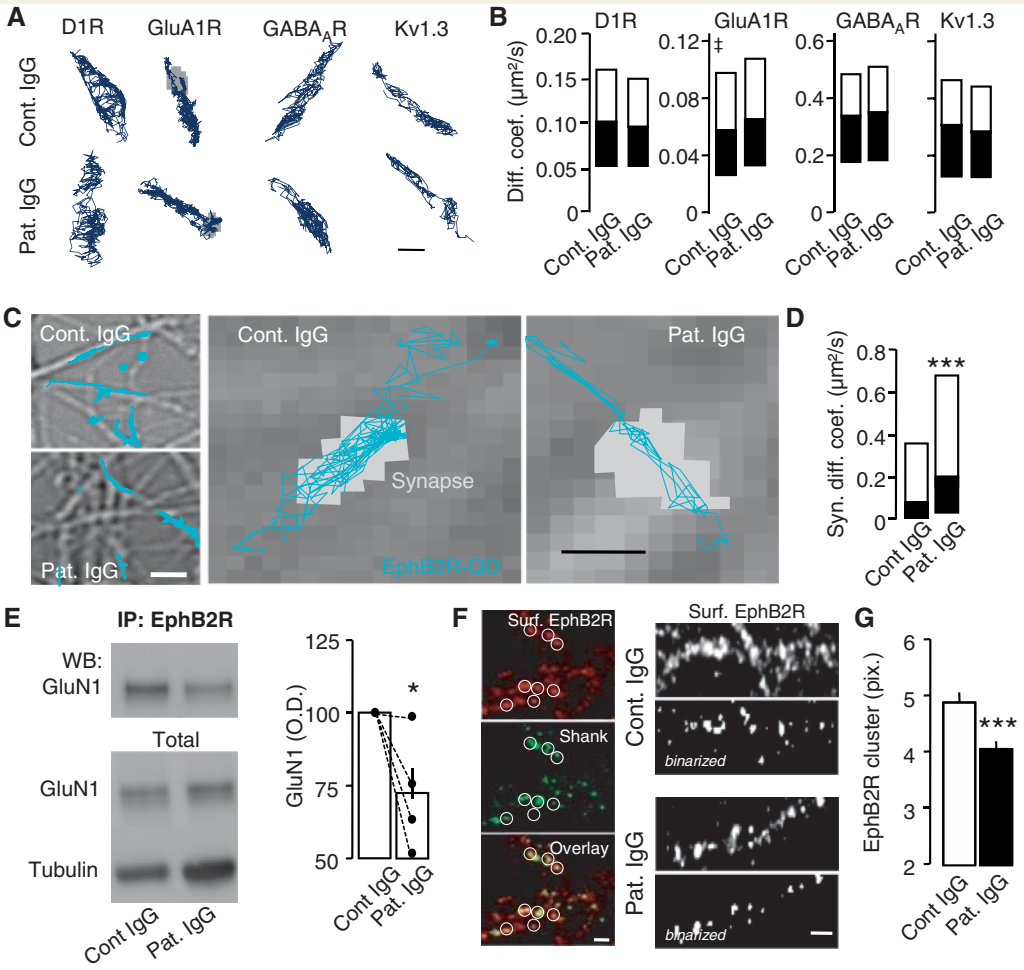

Figure 3 Patient IgG alters the EPHB2R surface diffusion and clustering by disturbing the interaction between surface GluN2A-NMDA receptor and EPHB2R. (**A**) Representative trajectories of surface dopamine D1 receptor, GluA1-AMPAR, α2-GABA$_A$R and potassium channel Kv1.3 (1000 frames, 50 ms acquisition) in neurons incubated with either control or patient IgG during 2 h. Glutamate synapses correspond to grey areas. Scale bar = 500 nm. (**B**) The instantaneous diffusion coefficient distributions (median ± 25–75% IQR) of dopamine D1 receptor, GluA1-AMPAR, α2-GABA$_A$R and potassium channel Kv1.3 in Control SNP793 or Patient 09-052 IgGs (control D1 receptor: median = 9×10^{-2} μm^2/s, 25–75% = 5×10^{-2}–$1 \times 5 \times 10^{-1}$ μm^2/s, n = 1639 trajectories; patient D1 receptor: median = 1×10^{-1} μm^2/s, 25–75% = 5×10^{-2}–15×10^{-2} μm^2/s, n = 1295, $P > 0.05$; control GluA1: median = 5×10^{-2} μm^2/s, 25–75% = 3×10^{-2}–9×10^{-2} μm^2/s, n = 2679; patient GluA1: median = 6×10^{-2} μm^2/s, 25–75% = 3×10^{-2}–12×10^{-1} μm^2/s, n = 2780; ‡$P < 0.001$; control α2-GABA$_A$R: median = 0.36 μm^2/s, 25–75% = 0.19–0.5 μm^2/s, n = 1639 trajectories; patient α2-GABA$_A$R: median = 0.34 μm^2/s, 25–75% = 0.19–0.48 μm^2/s, n = 1639 trajectories, $P > 0.05$; control Kv1.3: median = 0.31 μm^2/s, 25–75% = 0.18–0.43 μm^2/s, n = 1047 trajectories; patient Kv1.3: median = 0.32 μm^2/s, 25–75% = 0.18–0.45 μm^2/s, n = 734 trajectories, $P > 0.05$). (**C**) Representative trajectories of surface EPHB2R (blue lines, 1000 frames, 50 ms acquisition, scale bar = 5 μm) and enlarged trajectories (*right* panels) of surface EPHB2R within or outside synapses (grey areas) in neurons incubated with either Control SNP793 or Patient 09-052 IgGs during 2 h. Scale bar = 400 nm. (**D**) Synaptic surface diffusion of EPHB2 receptor significantly increased in the presence of patient IgG (n = 290) when compared with control IgG (n = 240) ($P < 0.001$). (**E**) Representative immunoblots showing the immunoprecipitation (IP) of EPHB2R with the GluN1 subunit in hippocampal cultures treated with either Control SNP793 or Patient 09-343 IgGs (*left* panel). The 'total' panel represents the total content of GluN1 and tubulin (input material) in control and patient conditions. *Right* panel: Patient IgGs reduced the optical density (O.D.) of GluN1 detection after EPHB2R immunoprecipitation when compared with control IgG conditions (n = 4 independent experiments). The immunoprecipitation amount signal was normalized to tubulin. (**F**) *Left:* Dendritic fragments from neurons incubated for 3 h either with Control SNP793, (5 μg/ml) or Patient 09-343, (5 μg/ml) IgGs and immunostained with surface EPHB2 receptors and postsynaptic density protein Shank. Overlay image shows high synaptic localization of surface EPHB2R. Scale bar = 10 μm. *Right* panels: Enlarged dendritic fragments of the raw surface EPHB2R detection (*top*) and binarized images (*bottom*), which highlight the EPHB2R surface clusters. Scale bar = 5 μm. (**G**) The size of the surface EPHB2R clusters was significantly reduced in a presence of patient IgG (n = 616 clusters) when compared with control IgG (n = 783 clusters). ***$P < 0.001$.

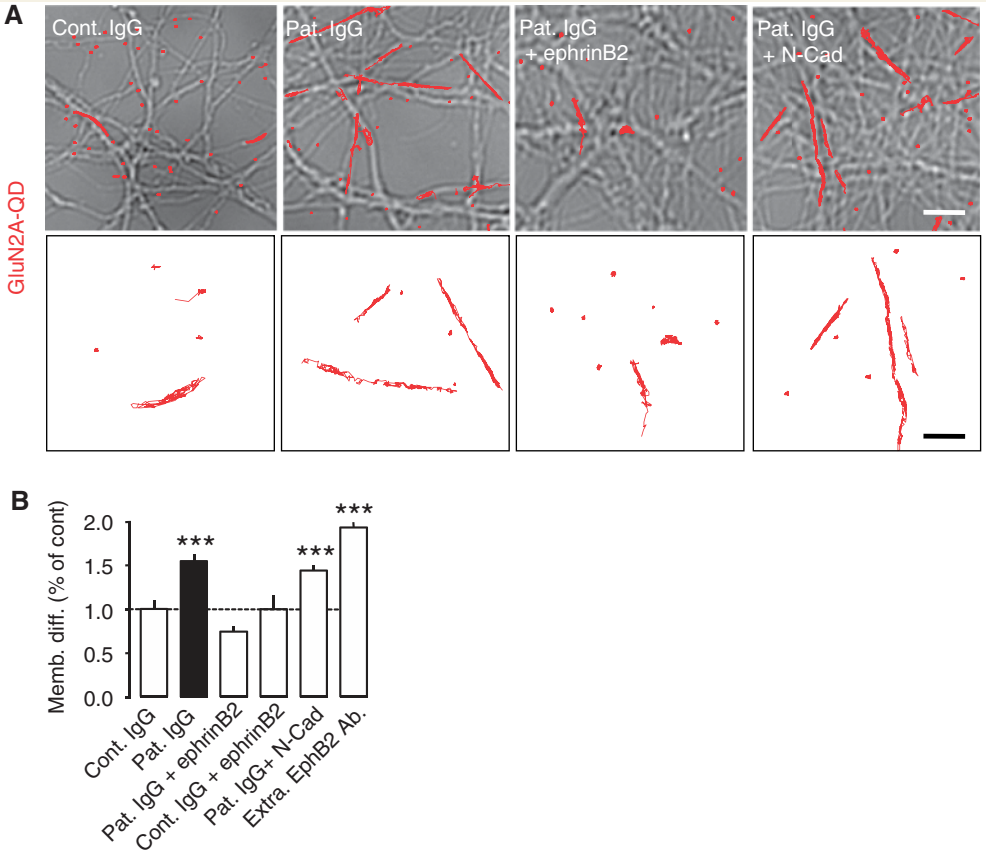

Figure 4 Patient IgG impact on GluN2A-NMDA receptor surface diffusion by disrupting NMDA receptor-EPHB2R interaction. (**A**) Representative trajectories of surface GluN2A-NMDA receptors (red lines, 1000 frames, 50 ms acquisition) in neurons incubated with either Control SNP793 IgG (5 μg/ml, 2 h), Patient 09-052 IgG (5 μg/ml, 2 h), patient IgG and ephrin-B2 ligand (Patient 09-052 IgG + ephrin-B2, 5 μg/ml, 2 h, ephrin-B2 ligand: 125 ng/ml), patient IgG and N-cadherin (Patient 09-052 IgG + N-cadherin, 5 μg/ml, 2 h; N-cadherin: 125 ng/ml). Scale bar = 10 μm. (**B**) Membrane instantaneous diffusion coefficient was significantly increased in the presence of patient IgG ($n = 743$ trajectories, $P < 0.001$), patient IgG with N-cadherin ($n = 2024$, $P < 0.001$), and antibodies against extracellular epitope of EPHB2R (Extra. EPHB2R Ab; EPHB2 antibody: 1 μg/ml, 2 h, $n = 1872$, $P < 0.001$) whereas it remained unaffected in patient IgG and ephrin-B2 ligand ($n = 764$, $P > 0.05$) or Control SNP793 IgG and ephrin-B2 ligand (5 μg/ml, 2 h, ephrin-B2 ligand: 125 ng/ml, $n = 164$, $P > 0.05$) conditions.

IgGs alone (Fig. 5E and F), Altogether, our findings confirm that patient IgG produced an internalization of NMDA receptors and further underline the role of the EPHB2R signalling in preventing this process.

To confirm these data in living animals, we injected in the dorsal hippocampus of adult mice controls or patient IgG (5–7 h incubation) in the presence or absence of ephrin-B2 ligand (Fig. 6A). As previously reported, injections of these IgGs in the brain of rats did not significantly alter the neuronal architecture (e.g. cell death rate) or the dendritic tree of pyramidal neurons (Hughes *et al.*, 2010). However, we observed that patient IgG reduced the surface staining (no permeabilization of the plasma membrane during immunohistochemical staining) of GluN1- (Fig. 6B and C) and GluN2A-NMDA receptors (Supplementary Fig. 5). Interestingly, this effect was partly reversed by the injection of ephrin-B2 ligands within the incubation period (Fig. 6B and C; Supplementary Fig. 5). Altogether, these data provide the first evidence that the deleterious effect of patient IgG on NMDA receptor surface dynamics and content can be pharmacologically prevented, both *in vitro* and *in vivo*, by ephrin-B2 stimulation of EPHB2R and/or the formation of ephrin-B2–EPHB2R complexes.

Discussion

The NMDA receptor plays a key role in several synaptic adaptation processes and dysfunctions of its signalling have been proposed as a core mechanism in several neurological disorders. Using high-resolution single nanoparticle imaging, we demonstrate that IgGs from patients with encephalitis and auto-NMDA antibodies, which cause neuropsychiatric symptoms in a reversible and titre-dependent manner, produce a differential effect on the two main GluN2A and GluN2B-containing NMDA receptor subtypes (Fig. 7). In the synapse, patient IgG induces a rapid dispersal of GluN2A-NMDA receptors, preventing their dynamic synaptic retention through the blockade of the interaction between

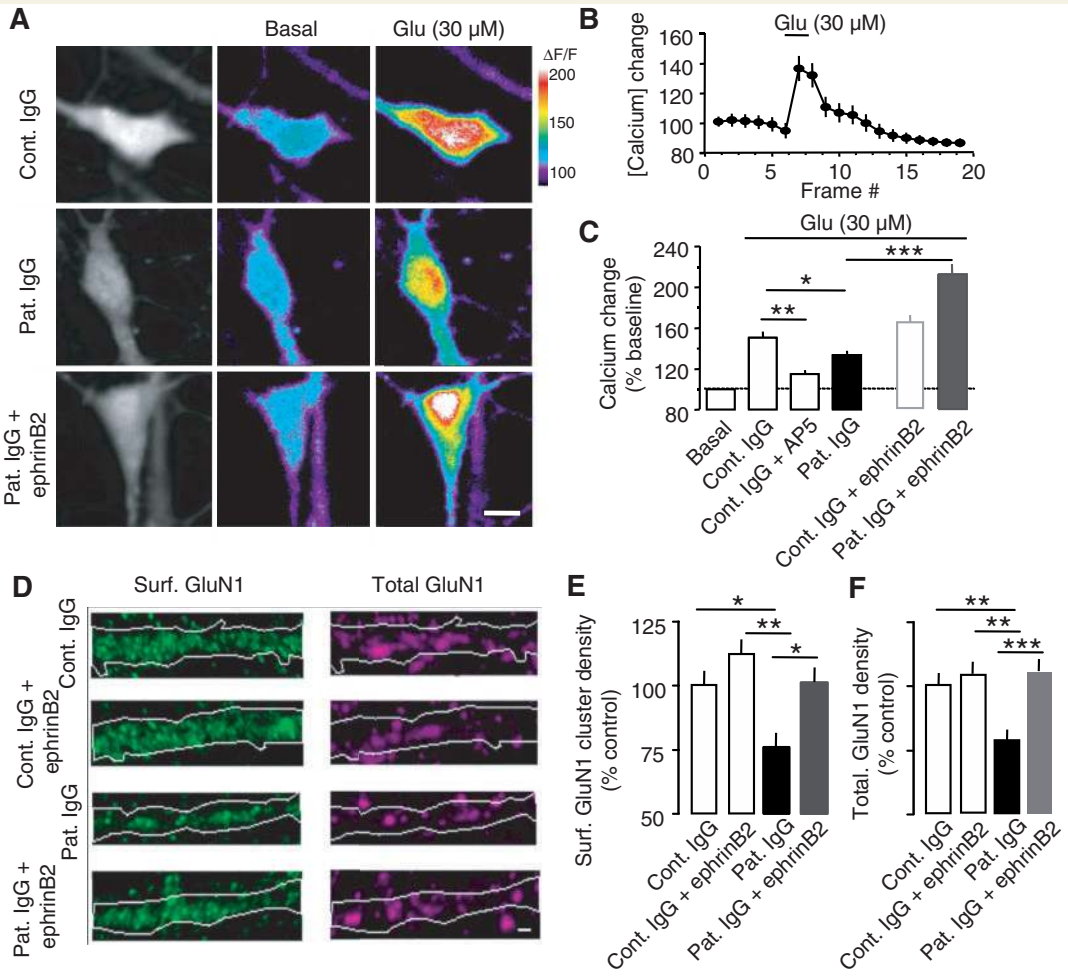

Figure 5 Ephrin-B2 ligand-induced activation of EPHB2R reverses the effect of patient IgG on NMDA receptor function and cell surface expression. (**A**) Representative images of hippocampal neurons incubated 2–4 h either with control (5 μg/ml), patient IgG (5 μg/ml) or patient IgG and ephrin-B2 ligand (125 ng/ml, 45 min) under the basal conditions or after glutamate (30 μM) stimulation. The pseudocolour representation shows the different intensity levels of the calcium indicator (Fluo4, 2 μM) before and after the glutamate stimulation. Scale bar = 20 μm. (**B**) Representative quantification of calcium intensity change ($\Delta F/F$) after the glutamate stimulation of the hippocampal neuron in the presence of control IgG. (**C**) Relative comparison (per cent of basal) of a transient calcium rise induced by glutamate in neurons treated with control IgG ($n = 57$ neurons), patient IgG ($n = 55$), control IgG and ephrin-B2 ligand ($n = 76$), patient IgG and ephrin-B2 ligand ($n = 108$). The transient calcium rise was blocked in control condition by AP-5 (10 μM) ($n = 22$). (**D**) Representative images of hippocampal neurons treated for 20 h with Control SNP793 IgG (7 μg/ml, *top row*), control IgG + ephrin-B2 ligand (*second row*), Patient 10-630 IgG (7 μg/ml, *third row*), patient IgG + ephrin-B2 ligand (*bottom*) and immunostained for both surface NMDA GluN1 (green) and internalized NMDA GluN1 (purple). Scale bar = 1 μm. (**E** and **F**) Quantitative comparison (per cent of control) of surface (**E**) and total (**F**) NMDA GluN1 cluster density between treatments, i.e. control IgG ($n = 13$ neurons), control IgG + ephrin-B2 ligand ($n = 10$ neurons), patient IgG ($n = 14$ neurons), patient IgG + ephrin-B2 ligand ($n = 15$ neurons). Surface and total GluN1 cluster densities were significantly decreased in the presence of patient IgG compared with control IgG ($n = 14$ and 13, $^*P < 0.05$; and $n = 14$ and 13, $^{**}P < 0.01$, respectively), whereas such a decrease was prevented in the condition in which patient IgG and clustered ephrin were applied. Values represent the mean ± SEM.

extracellular domains of GluN1/2 subunits and EPHB2R (Dalva *et al*., 2000, 2007). In contrast, GluN2B-NMDA receptor dynamics were highly reduced in the extrasynaptic area, consistent with an antibody-induced receptor cross-linking and subsequent receptor endocytosis (Hughes *et al*., 2010). Functionally, these drastic changes in GluN2-NMDA receptor surface dynamics abolished synaptic plasticity although the trafficking of other membrane receptors and channels, e.g. dopamine D1 receptor, $GABA_AR$, Kv1.3 and AMPAR, remained mostly unaffected. Together, these data support a model in which the extracellular domain of NMDA receptors, which is the target in some patients with autoimmune antibody-induced neurological symptoms, plays an important role in the synaptic retention of NMDA receptors and in plasticity processes. Once the receptors escape the postsynaptic densities, they are extrasynaptically endocytosed in a GluN2 subunit-independent manner. Thus, the regulation of NMDA receptor

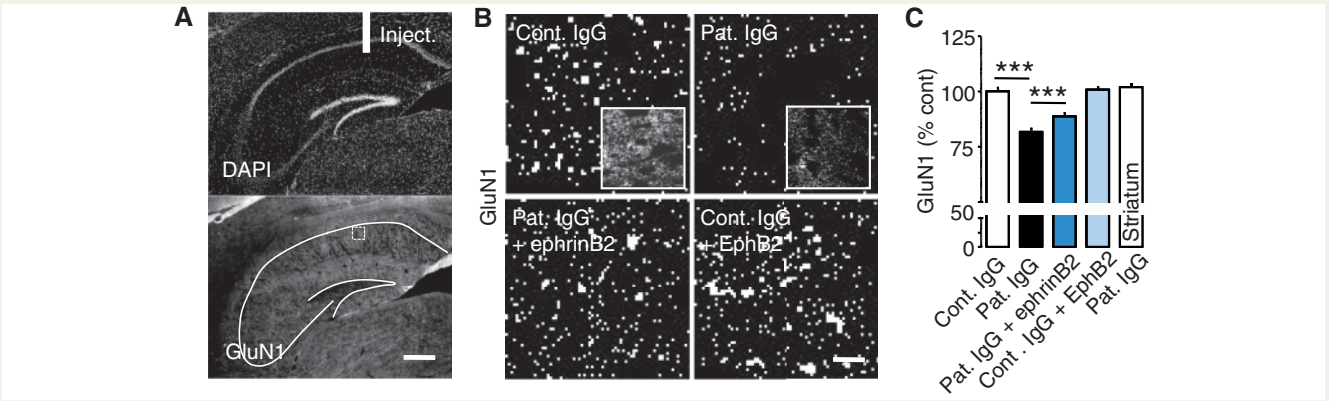

Figure 6 Injection of EPHrinB2 ligand *in vivo* reverses the effect of patient IgG on NMDA receptor cell surface expression. (**A**) Patient IgGs were injected in the dorsal hippocampus of FVB mice and 5–7 h after the injection, surface GluN1 subunits were immunostained (*lower* panel). Scale bar = 400 μm. (**B**) Surface staining of GluN1 subunits in the CA1 area (stratum radiatum) of mice injected with either Control SNP793 IgG (1 mg/ml), Patient 09-052 IgG (1 mg/ml), Patient 09-052 IgG (1 mg/ml) + ephrin-B2 ligand (25 μg/ml) or Control SNP793 IgG (1 mg/ml) + ephrin-B2 ligand (25 μg/ml). GluN1 subunit clusters were observed and binarized on the images. Scale bar = 20 μm. (**C**) Relative comparison (per cent of control, 2–5 mice per group) of GluN1 subunit surface staining between control IgG ($n = 629$ clusters, $n = 4$ mice), patient IgG ($n = 826$ clusters, $n = 5$ mice), patient IgG and ephrin-B2 ligand ($n = 810$ clusters, $n = 3$ mice) or control IgG and ephrin-B2 ligand ($n = 863$ clusters, $n = 2$ mice) or patient IgG in the striatum ($n = 1063$ clusters, $n = 5$ mice). Note the significant difference in cluster intensity between groups (***$P < 0.001$).

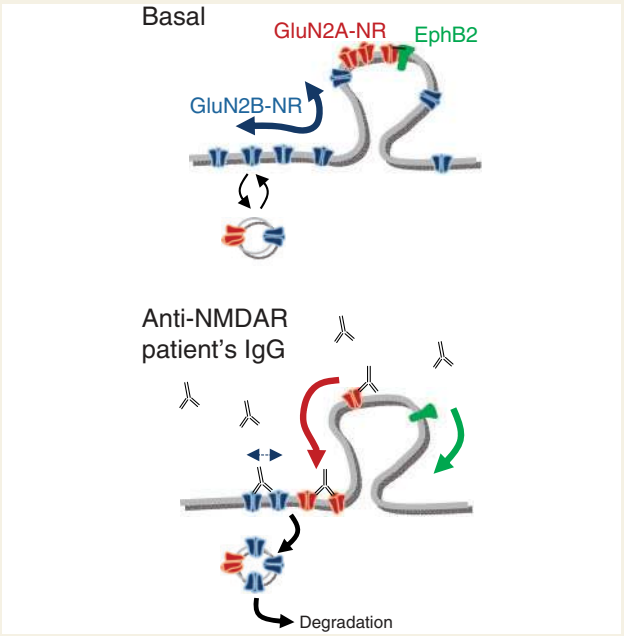

Figure 7 Proposed model of the impact of anti-NMDA receptor patient IgG on GluN2A- and GluN2B-NMDA receptor trafficking. In basal conditions, GluN2A-NMDA receptors are actively anchored in synapses in which their diffusion is rather restrained. GluN2B-NMDA receptors are more extrasynaptic and explore large dendritic areas. The patient IgG target extracellular domains of the GluN-NMDA receptors preventing the interaction between NMDA receptors and EPHB2R in the synaptic area. In the extrasynaptic compartment, patient IgG dramatically reduces the surface diffusion of NMDA receptors, likely favouring their internalization and degradation.

surface trafficking emerges as a crucial cellular pathway involved in the pathophysiological tuning of excitatory synapse transmission.

Former pioneer studies have revealed that patient anti-NMDA receptor IgG targets surface GluN1-NMDA receptors and causes a selective and reversible decrease in GluN1-NMDA receptor surface density and synaptic localization (Dalmau *et al.*, 2008; Hughes *et al.*, 2010). The mechanism of this decrease was probably dependent on NMDA receptor internalization (Hughes *et al.*, 2010), which occurs mostly outside synapses (Blanpied *et al.*, 2002; Petralia *et al.*, 2003). Although these immunohistochemical and electrophysiological studies undoubtedly provide key information on the overall impact of patient anti-NMDA receptor IgG on NMDA receptor distribution, the spatial and time resolutions of these approaches did not provide insights into the molecular dynamics of the antibodies' surface targets, particularly in compartments with sub-wavelength sizes (e.g. synapse). Indeed, the detection threshold of classical immunocytochemical approaches is rather high (~>250 nm in classical live imaging microscopy) and does not permit the investigation of single receptor diffusion since it detects only receptor populations. To overcome these limitations, we used real-time single particle tracking and imaging to elucidate the cellular pathways involving the IgGs of NMDA receptor encephalitis on NMDA receptor dysfunctions. Interestingly, quantum dot–receptor complex tracking can be performed over a long period of time in comparison with standard organic fluorophore–receptor complexes since quantum dots are photostable and do not photobleach (Dahan *et al.*, 2003; Groc *et al.*, 2004, 2007*b*). In addition, because quantum dots are smaller than the diffraction limits of an optical microscope, its image corresponds to a spread point function that can be fitted by a 2D Gaussian approximation. Consequently, quantum dot position could then be

determined with a point accuracy of ~30 nm (Groc *et al*., 2007*b*; Triller and Choquet, 2008), providing a rather unique way of exploring the lateral movement of single receptors in confined compartments with sub-wavelength precision (Triller and Choquet, 2005; Groc *et al*., 2007*b*). Using this approach, we demonstrate that patient anti-NMDA receptor IgGs impact, in opposite manner, on the surface dynamics of synaptic GluN2A-NMDA receptors and extrasynaptic GluN2B-NMDA receptors. In the basal condition, surface GluN2B-NMDA receptors are quite dynamic and explore a large area of the dendritic tree (Groc *et al*., 2006; Bard *et al*., 2010). In the presence of patient anti-NMDA receptor IgGs, their diffusion was massively reduced, consistent with previously described antibody-induced cross-linking of surface receptors (Groc *et al*., 2008; Heine *et al*., 2008). In addition, this reduced surface diffusion in the extrasynaptic compartment likely results from an increase in endocytosis of the receptors (Tardin *et al*., 2003). For synaptic GluN2A-NMDA receptors, the effect of patient anti-NMDA receptor IgG was strikingly different. In the basal conditions, GluN2A-NMDA receptors directly interact with intracellular PDZ domain-containing scaffold proteins (Lau and Zukin, 2007) and transmembrane EPHB2Rs (Dalva *et al*., 2000), leading to a high synaptic retention of NMDA receptors. Surprisingly, patient anti-NMDA receptor IgG did not further stabilize GluN2A-NMDA receptors through a cross-linking process, but rather destabilized them by preventing their extracellular association with EPHB2R. It should be noted that these data do not rule out the possibility that patient anti-NMDA receptor IgGs also alter the interaction between the extracellular domain of NMDA receptors with other direct interactors, e.g. the neuropilin tolloid-like 1 transmembrane protein (Neto1) (Ng *et al*., 2009). Together, the spatial and temporal resolutions of single particle tracking provided a unique way to unravel the molecular and cellular dynamics of the membrane targets of patient anti-NMDA receptor IgG, and actually delineated a new strategy to balance NMDA receptor dysfunction in patients with NMDA receptor autoantibody encephalitis.

The presence of NMDA receptor autoantibodies has also been reported in systemic lupus erythematosus (Lee *et al*., 2009). In children, whose mothers suffer from systemic lupus erythematosus, NMDA receptor autoantibodies are suspected to cause multiple neurological and psychiatric disorders, such as congenital brain injuries, long-term cognitive deficits, psychosis, abnormal movements and respiratory failure. Although the origin is still unclear, these deficits can be triggered during the embryonic period of brain development by NMDA receptor autoantibodies in maternal circulation since the blood–brain barrier is not fully formed *in utero* (Lee *et al*., 2009). In this developmental framework, most of the effects of the NMDA receptor autoantibodies are likely due to the targeting of GluN2B-NMDA receptors since they are predominant in the embryonic and early postnatal periods (Monyer *et al*., 1994). In mature hippocampal networks, we show that both GluN2A- and GluN2B-NMDA receptor trafficking are affected by NMDA receptor autoantibodies, suggesting as previously reported (Dalmau *et al*., 2008) that the targeting is the GluN1 subunit and not GluN2A or 2B subunits. Consistently, the interaction of EPHB2R and NMDA receptors, which is disrupted by NMDA receptor autoantibodies, is mediated by an extracellular domain of GluN1 subunit (Dalva *et al*., 2000). In the presence of NMDA receptor autoantibodies, the lateral escape of synaptic NMDA receptors, which are composed of a mixture of GluN2A-NMDA receptors and GluN1-GluN2A-GluN2B-NMDA receptors (Kohr, 2006), would thus result from the lack of interaction with stable synaptic interacter/anchor (e.g. EPHB2R). In the extrasynaptic compartment, NMDA receptor autoantibodies are likely to induce cross-linking of GluN-NMDA receptors, favouring their internalization and degradation. In contrast, when the NMDA receptor/EPHB2R interaction was induced by stimulation with ephrin-B2 ligands, NMDA receptors were more efficiently anchored in synapses and less sensitive to NMDA receptor autoantibodies. Among the various questions that such a discovery brings to our attention, one should be mentioned. It has been proposed that major neurological disorders (e.g. Huntington disease, ischaemia) result from an altered activation and/or trafficking of NMDA receptors. To date, trials that aim at preventing NMDA receptor dysfunction in such human disorders and their related animal models have, however, not reach our level of expectation since most of these drugs are not specific for a subtype of NMDA receptor (Javitt, 2004). Based on this study, it further emerges that rather than acting directly on the NMDA receptor channel or its activity, the development of molecules that will impact on NMDA receptor surface trafficking and synaptic retention may represent a potentially relevant strategy to balance NMDA receptor dysfunction in complex neurological disorders. As demonstrated earlier, ephrin-B2–EPHB2R-dependent signalling is a promising target, paving the way for the discovery of other relevant molecules.

In conclusion, the identification of the cellular pathways involved in such anti-NMDA receptor autoimmune disorders sheds new light on how neuronal communication can be preserved in severe neurological and psychiatric disorders involving NMDA receptor dysfunction. It further demonstrates how single nanoparticle tracking can be a powerful approach to dissect molecular and cellular cascades and isolate new therapeutic targets. It clearly points toward an extracellular regulation of the NMDA receptor trafficking in an acute model of encephalitis, consistent with the emerging role of the relationship between the extracellular matrix and the NMDA receptor surface trafficking (Groc *et al*., 2007*a*; Michaluk *et al*., 2009). Dysfunctions of NMDA receptor signalling are involved in several major neurological and psychiatric disorders and, although different primary intracellular or extracellular triggers may be involved in different pathologies, these may share downstream molecular cascades that lead to weak NMDA receptor synaptic retention and altered surface dynamics.

Acknowledgements

We thank the patients for their participation, Christelle Breillat and Naura Chounlamountri for cell culture assistance, Philippe Legros, Christel Poujol (BIC Bordeaux) and Matthieu Sainlos for technical assistance and lab members for constructive discussions. Blood and CSF samples were collected with the help of Neurobiotec Bank and the Hospices Civils de Lyon.

Funding

Agence Nationale de la Recherche (NMDASurf to L.G.); Centre National de la Recherche Scientifique; Institut National de la santé et de la Recherche Médicale; Conseil Régional d'Aquitaine and Bya Grant of the French Ministry of Health.

Supplementary material

Supplementary material is available at *Brain* online.

References

Ashby MC, Ibaraki K, Henley JM. It's green outside: tracking cell surface proteins with pH-sensitive GFP. Trends Neurosci 2004; 27: 257–61.

Bannai H, Levi S, Schweizer C, Inoue T, Launey T, Racine V, et al. Activity-dependent tuning of inhibitory neurotransmission based on GABAAR diffusion dynamics. Neuron 2009; 62: 670–82.

Bard L, Groc L. Glutamate receptor dynamics and protein interaction: lessons from the NMDA receptor. Mol Cell Neurosci 2011; 48: 298–307.

Bard L, Sainlos M, Bouchet D, Cousins S, Mikasova L, Breillat C, et al. Dynamic and specific interaction between synaptic NR2-NMDA receptor and PDZ proteins. Proc Natl Acad Sci USA 2010; 107: 19561–6.

Blanpied TA, Scott DB, Ehlers MD. Dynamics and regulation of clathrin coats at specialized endocytic zones of dendrites and spines. Neuron 2002; 36: 435–49.

Chapman MR, Vause HE. Anti-NMDA receptor encephalitis: diagnosis, psychiatric presentation, and treatment. Am J Psychiatry 2011; 168: 245–51.

Cull-Candy SG, Leszkiewicz DN. Role of distinct NMDA receptor subtypes at central synapses. Sci STKE 2004; 2004: re16.

Dahan M, Levi S, Luccardini C, Rostaing P, Riveau B, Triller A. Diffusion dynamics of glycine receptors revealed by single-quantum dot tracking. Science 2003; 302: 442–5.

Dalmau J, Gleichman AJ, Hughes EG, Rossi JE, Peng X, Lai M, et al. Anti-NMDA-receptor encephalitis: case series and analysis of the effects of antibodies. Lancet Neurol 2008; 7: 1091–8.

Dalmau J, Lancaster E, Martinez-Hernandez E, Rosenfeld MR, Balice-Gordon R. Clinical experience and laboratory investigations in patients with anti-NMDA receptor encephalitis. Lancet Neurol 2011; 10: 63–74.

Dalmau J, Tuzun E, Wu HY, Masjuan J, Rossi JE, Voloschin A, et al. Paraneoplastic anti-N-methyl-D-aspartate receptor encephalitis associated with ovarian teratoma. Ann Neurol 2007; 61: 25–36.

Dalva MB, McClelland AC, Kayser MS. Cell adhesion molecules: signalling functions at the synapse. Nat Rev Neurosci 2007; 8: 206–20.

Dalva MB, Takasu MA, Lin MZ, Shamah SM, Hu L, Gale NW, et al. EphB receptors interact with NMDA receptors and regulate excitatory synapse formation. Cell 2000; 103: 945–56.

Groc L, Choquet D, Chaouloff F. The stress hormone corticosterone conditions AMPAR surface trafficking and synaptic potentiation. Nat Neurosci 2008; 11: 868–70.

Groc L, Choquet D, Stephenson FA, Verrier D, Manzoni OJ, Chavis P. NMDA receptor surface trafficking and synaptic subunit composition are developmentally regulated by the extracellular matrix protein Reelin. J Neurosci 2007a; 27: 10165–75.

Groc L, Lafourcade M, Heine M, Renner M, Racine V, Sibarita JB, et al. Surface trafficking of neurotransmitter receptor: comparison between single-molecule/quantum dot strategies. J Neurosci 2007b; 27: 12433–7.

Groc L, Heine M, Cognet L, Brickley K, Stephenson FA, Lounis B, et al. Differential activity-dependent regulation of the lateral mobilities of AMPA and NMDA receptors. Nat Neurosci 2004; 7: 695–6.

Groc L, Heine M, Cousins SL, Stephenson FA, Lounis B, Cognet L, et al. NMDA receptor surface mobility depends on NR2A-2B subunits. Proc Natl Acad Sci USA 2006; 103: 18769–74.

Heine M, Groc L, Frischknecht R, Beique JC, Lounis B, Rumbaugh G, et al. Surface mobility of postsynaptic AMPARs tunes synaptic transmission. Science 2008; 320: 201–5.

Henderson JT, Georgiou J, Jia Z, Robertson J, Elowe S, Roder JC, et al. The receptor tyrosine kinase EphB2 regulates NMDA-dependent synaptic function. Neuron 2001; 32: 1041–56.

Hughes EG, Peng X, Gleichman AJ, Lai M, Zhou L, Tsou R, et al. Cellular and synaptic mechanisms of anti-NMDA receptor encephalitis. J Neurosci 2010; 30: 5866–75.

Irani SR, Alexander S, Waters P, Kleopa KA, Pettingill P, Zuliani L, et al. Antibodies to Kv1 potassium channel-complex proteins leucine-rich, glioma inactivated 1 protein and contactin-associated protein-2 in limbic encephalitis, Morvan's syndrome and acquired neuromyotonia. Brain 2010; 133: 2734–48.

Javitt DC. Glutamate as a therapeutic target in psychiatric disorders. Mol Psychiatry 2004; 9: 984–97, 979.

Kohr G. NMDA receptor function: subunit composition versus spatial distribution. Cell Tissue Res 2006; 326: 439–46.

Lai M, Hughes EG, Peng X, Zhou L, Gleichman AJ, Shu H, et al. AMPA receptor antibodies in limbic encephalitis alter synaptic receptor location. Ann Neurol 2009; 65: 424–34.

Lai M, Huijbers MG, Lancaster E, Graus F, Bataller L, Balice-Gordon R, et al. Investigation of LGI1 as the antigen in limbic encephalitis previously attributed to potassium channels: a case series. Lancet Neurol 2010; 9: 776–85.

Lancaster E, Huijbers MG, Bar V, Boronat A, Wong A, Martinez-Hernandez E, et al. Investigations of caspr2, an autoantigen of encephalitis and neuromyotonia. Ann Neurol 2011a; 69: 303–11.

Lancaster E, Martinez-Hernandez E, Titulaer MJ, Boulos M, Weaver S, Antoine JC, et al. Antibodies to metabotropic glutamate receptor 5 in the Ophelia syndrome. Neurology 2011b; 77: 1698–701.

Lancaster E, Lai M, Peng X, Hughes E, Constantinescu R, Raizer J, et al. Antibodies to the GABA(B) receptor in limbic encephalitis with seizures: case series and characterisation of the antigen. Lancet Neurol 2010; 9: 67–76.

Lau CG, Zukin RS. NMDA receptor trafficking in synaptic plasticity and neuropsychiatric disorders. Nat Rev Neurosci 2007; 8: 413–26.

Lebas A, Husson B, Didelot A, Honnorat J, Tardieu M. Expanding spectrum of encephalitis with NMDA receptor antibodies in young children. J Child Neurol 2010; 25: 742–5.

Lee JY, Huerta PT, Zhang J, Kowal C, Bertini E, Volpe BT, et al. Neurotoxic autoantibodies mediate congenital cortical impairment of offspring in maternal lupus. Nat Med 2009; 15: 91–6.

Lim IA, Hall DD, Hell JW. Selectivity and promiscuity of the first and second PDZ domains of PSD-95 and synapse-associated protein 102. J Biol Chem 2002; 277: 21697–711.

Lippincott-Schwartz J, Patterson GH. Development and use of fluorescent protein markers in living cells. Science 2003; 300: 87–91.

Lu J, Helton TD, Blanpied TA, Racz B, Newpher TM, Weinberg RJ, et al. Postsynaptic positioning of endocytic zones and AMPA receptor cycling by physical coupling of dynamin-3 to Homer. Neuron 2007; 55: 874–89.

Lu W, Man H, Ju W, Trimble WS, MacDonald JF, Wang YT. Activation of synaptic NMDA receptors induces membrane insertion of new AMPA receptors and LTP in cultured hippocampal neurons. Neuron 2001; 29: 243–54.

Manto M, Dalmau J, Didelot A, Rogemond V, Honnorat J. In vivo effects of antibodies from patients with anti-NMDA receptor encephalitis: further evidence of synaptic glutamatergic dysfunction. Orphanet J Rare Dis 2010; 5: 31.

Manto MU, Laute MA, Aguera M, Rogemond V, Pandolfo M, Honnorat J. Effects of anti-glutamic acid decarboxylase antibodies

associated with neurological diseases. Ann Neurol 2007; 61: 544–51.
Mas N, Saiz A, Leite MI, Waters P, Baron M, Castano D, et al. Antiglycine-receptor encephalomyelitis with rigidity. J Neurol Neurosurg Psychiatry 2011; 82: 1399–401.
Michaluk P, Mikasova L, Groc L, Frischknecht R, Choquet D, Kaczmarek L. Matrix metalloproteinase-9 controls NMDA receptor surface diffusion through integrin beta1 signaling. J Neurosci 2009; 29: 6007–12.
Monyer H, Burnashev N, Laurie DJ, Sakmann B, Seeburg PH. Developmental and regional expression in the rat brain and functional properties of four NMDA receptors. Neuron 1994; 12: 529–40.
Morris RG. Elements of a neurobiological theory of hippocampal function: the role of synaptic plasticity, synaptic tagging and schemas. Eur J Neurosci 2006; 23: 2829–46.
Moscato EH, Jain A, Peng X, Hughes EG, Dalmau J, Balice-Gordon RJ. Mechanisms underlying autoimmune synaptic encephalitis leading to disorders of memory, behavior and cognition: insights from molecular, cellular and synaptic studies. Eur J Neurosci 2010; 32: 298–309.
Ng D, Pitcher GM, Szilard RK, Sertie A, Kanisek M, Clapcote SJ, et al. Neto1 is a novel CUB-domain NMDA receptor-interacting protein required for synaptic plasticity and learning. PLoS Biol 2009; 7: e41.
Nolt MJ, Lin Y, Hruska M, Murphy J, Sheffler-Colins SI, Kayser MS, et al. EphB controls NMDA receptor function and synaptic targeting in a subunit-specific manner. J Neurosci 2011; 31: 5353–64.
Park M, Penick EC, Edwards JG, Kauer JA, Ehlers MD. Recycling endosomes supply AMPA receptors for LTP. Science 2004; 305: 1972–5.
Park M, Salgado JM, Ostroff L, Helton TD, Robinson CG, Harris KM, et al. Plasticity-induced growth of dendritic spines by exocytic trafficking from recycling endosomes. Neuron 2006; 52: 817–30.
Petralia RS, Wang YX, Wenthold RJ. Internalization at glutamatergic synapses during development. Eur J Neurosci 2003; 18: 3207–17.
Tai CY, Kim SA, Schuman EM. Cadherins and synaptic plasticity. Curr Opin Cell Biol 2008; 20: 567–75.
Tardin C, Cognet L, Bats C, Lounis B, Choquet D. Direct imaging of lateral movements of AMPA receptors inside synapses. EMBO J 2003; 22: 4656–65.
Tovar KR, Westbrook GL. The incorporation of NMDA receptors with a distinct subunit composition at nascent hippocampal synapses in vitro. J Neurosci 1999; 19: 4180–8.
Triller A, Choquet D. Surface trafficking of receptors between synaptic and extrasynaptic membranes: and yet they do move! Trends Neurosci 2005; 28: 133–9.
Triller A, Choquet D. New concepts in synaptic biology derived from single-molecule imaging. Neuron 2008; 59: 359–74.
Vincent A, Irani SR, Lang B. The growing recognition of immunotherapy-responsive seizure disorders with autoantibodies to specific neuronal proteins. Curr Opin Neurol 2010; 23: 144–50.
Wang Z, Edwards JG, Riley N, Provance DW Jr, Karcher R, Li XD, et al. Myosin Vb mobilizes recycling endosomes and AMPA receptors for postsynaptic plasticity. Cell 2008; 135: 535–48.
Wenthold RJ, Prybylowski K, Standley S, Sans N, Petralia RS. Trafficking of NMDA receptors. Annu Rev Pharmacol Toxicol 2003; 43: 335–58.
Yashiro K, Philpot BD. Regulation of NMDA receptor subunit expression and its implications for LTD, LTP, and metaplasticity. Neuropharmacology 2008; 55: 1081–94.
Zhang Q, Tanaka K, Sun P, Nakata M, Yamamoto R, Sakimura K, et al. Suppression of synaptic plasticity by cerebrospinal fluid from anti-NMDA receptor encephalitis patients. Neurobiol Dis 2012; 45: 610–5.